

Intrinsic magnetic properties of the superconductor $\text{NdFeAsO}_{0.9}\text{F}_{0.1}$ from local and global measurements

R Prozorov¹, M E Tillman, E D Mun and P C Canfield

Ames Laboratory and Department of Physics & Astronomy,
Iowa State University, Ames, IA 50011
E-mail: prozorov@ameslab.gov

New Journal of Physics **11** (2009) 035004 (9pp)

Received 6 January 2009

Published 25 March 2009

Online at <http://www.njp.org/>

doi:10.1088/1367-2630/11/3/035004

Abstract. Magneto-optical imaging was used to study the local magnetization in polycrystalline $\text{NdFeAsO}_{0.9}\text{F}_{0.1}$ (NFAOF). Individual crystallites up to $\sim 200 \times 100 \times 30 \mu\text{m}^3$ in size could be mapped at various temperatures. The in-grain, persistent current density is about $j \sim 10^5 \text{ A cm}^{-2}$ and the magnetic relaxation rate in a remanent state peaks at about $T_m \sim 38 \text{ K}$. By comparison with the total magnetization measured in a bar-shaped, dense, polycrystalline sample, we suggest that $\text{NdFeAsO}_{0.9}\text{F}_{0.1}$ is similar to high- T_c cuprates, in between $\text{Bi}_2\text{Sr}_2\text{CaCu}_2\text{O}_{8+x}$ and $\text{YBa}_2\text{Cu}_3\text{O}_{7-x}$ in terms of the vortex response in the mixed state. We find an apparent crossover in the pinning strength at $\sim 38 \text{ K}$ that could be associated either with vortex decoupling or melting. Below this temperature the static and dynamic vortex behavior is consistent with the collective pinning and creep.

Contents

1. Introduction	2
2. Experimental	2
3. Results and discussion	3
3.1. Direct visualization of the magnetic flux	3
3.2. Supercurrent density	5
3.3. Magnetic relaxation	6
4. Conclusions	8
Acknowledgments	8
References	9

¹ Author to whom any correspondence should be addressed.

1. Introduction

The recently discovered rare earth iron oxypnictides represent a new class of layered, high- T_c superconductors [1]. Rich chemistry allows for both electron and hole doping [2] as well as magnetism coexisting with, and possibly enhancing, superconductivity. Large superconducting crystals based on the oxygen-free parent compounds AFe_2As_2 (122 system, where A is an alkaline earth element) can be grown in flux at ambient pressure (see e.g. A = Ba [3], Sr [4] and Ca [5]). A detailed investigation of both local and global vortex properties in a representative of the 122 system, $Ba(Fe_{0.93}Co_{0.07})_2As_2$ single crystals, was reported in [6] where surprising similarities to cuprate superconductors, such as fishtail magnetization, very fast relaxation rate and a crossover to the plastic flux creep, were found.

On the other hand the highest T_c pnictide superconductors are based on the $RFeAsO$ parent compounds (1111 system, where R is a rare earth element). Unfortunately, the same rich chemistry that allows for high T_c makes the growth of single crystals difficult and, so far, mostly polycrystalline samples exist with the exception of some small single crystals [7]. In this paper we report local and global properties of relatively large single crystals of Nd-1111 and show that this class of Fe-based pnictides also shows unconventional vortex behavior. $NdFeAsO_{0.9}F_{0.1}$ (NFAOF) with a transition temperature exceeding 51 K was reported in [8]. This and related materials with Sm and Pr have the highest ambient pressure T_c values and are also interesting because of the possible interplay of the local moment of the rare earth and superconductivity. Predictions have been made for vortex melting similar to $Bi_2Sr_2CaCu_2O_{8+x}$ (BSCCO-2212) [9] and quantum critical behavior [10]. NMR studies favor nodal superconductivity [11], infrared ellipsometry suggests large electromagnetic anisotropy [12] and evidence of electromagnetic granularity has also been reported [13]. The temperature-dependent anisotropy was reported in Nd- and Sm-1111 single crystals from torque measurements [14] and a similar behavior was inferred from the measurements of the first critical field in Pr-1111 crystals with a miniature Hall probe [16]. These observations prompt further investigation of similarities to high- T_c cuprates and/or other unconventional materials, such as two-gap MgB_2 .

In this paper we present detailed magnetization measurements on both single crystallite and bulk, polycrystalline NFAOF. These results provide clear insight into the mesoscopic and macroscopic behavior of the superconducting mixed state. NFAOF exhibits a fast non-monotonic magnetic relaxation of the vortex state that is strikingly similar to that associated with the 2D vortex melting found in BSCCO-2212, but NFAOF has much stronger interlayer coupling.

2. Experimental

The high-pressure synthesis of samples with a nominal composition of $NdFeAsO_{0.9}F_{0.1}$ was carried out in a cubic, multianvil apparatus, with an edge length of 19 mm from Rockland Research Corporation. Stoichiometric amounts of $NdFe_3As_3$, Nd_2O_3 , NdF_3 and Nd were pressed into a pellet with mass of approximately 0.5 g and placed inside of a BN crucible with an inner diameter of 5.5 mm. The synthesis was carried out at about 3.3 GPa. The temperature was increased over a period of one hour from 1350 to 1400 °C and held for 8 h before being quenched to room temperature. The pressure was then released and the sample removed mechanically. More details of the synthesis and characterization will be found elsewhere [17]. The value of 10% F substitution is nominal, based on the initial stoichiometry of the pellet.

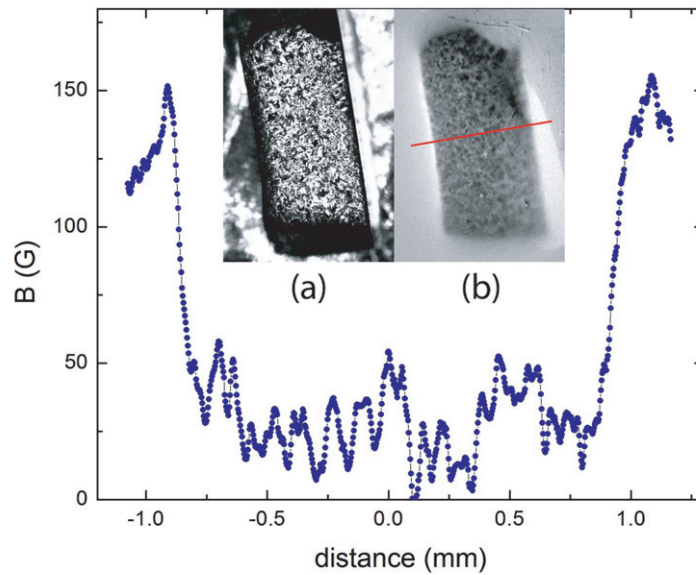


Figure 1. Main frame: Meissner screening of a 100 Oe field applied after zfc. $B(r)$ was taken along the line shown in inset (b). Inset (a): Optical image of the sample used in magnetometry and local studies. Inset (b): MO image of a 100 Oe field applied after zfc.

The synthesis yields polycrystalline $\text{NdFeAsO}_{0.9}\text{F}_{0.1}$ samples that contain what appears to be plate-like single crystals as large as $300\ \mu\text{m}$. Whereas extraction of these crystallites is difficult, we could measure properties of individual crystals by using local magneto-optical imaging. Comparing our observations with data from conventional magnetometry, we are able to provide in-depth magnetic characterization of these new superconductors. For the measurements of total magnetic moment, a slab-like sample that showed best overall screening and trapping of the magnetic flux was selected by using magneto-optical imaging. A *Quantum Design* MPMS magnetometer was used for the measurements of the total magnetic moment. Magneto-optical (MO) imaging was performed in a ^4He optical flow-type cryostat using Faraday rotation of polarized light in a Bi-doped iron-garnet film with an in-plane magnetization [18]. The spatial resolution of the technique is about $3\ \mu\text{m}$ with a sensitivity to magnetic field of about 1 G. The temporal resolution is about 30 ms.

3. Results and discussion

3.1. Direct visualization of the magnetic flux

We first examined morphological features visible in polarized-light and then established the correspondence between these features and the observed local magnetic behavior. Figure 1(a) shows the entire sample used in the comparative study. Figure 1(b) shows the MO image in a 100 Oe applied magnetic field obtained after zero-field cooling (zfc). There is Meissner screening, better seen in the magnetic induction profile shown in the main frame of figure 1 taken along the line shown in figure 1(b). Figures 2(a) and (d) show two different regions of the polished sample and provide clear evidence of well-faceted crystallites with cross-sections as

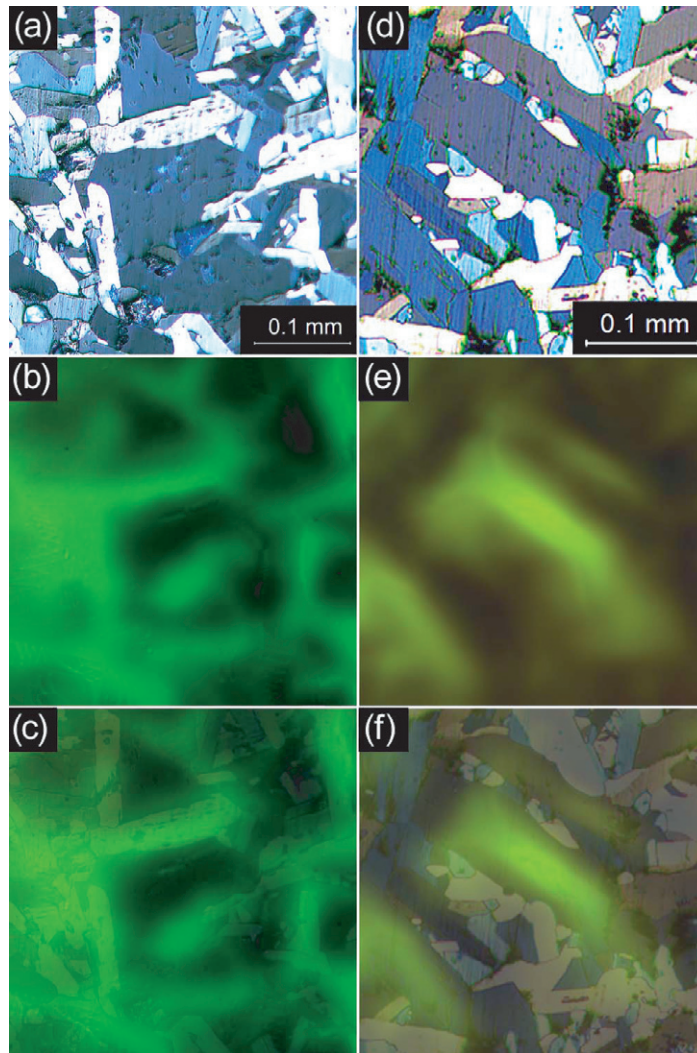


Figure 2. (a) Polarized-light image of part of the polished sample surface. (b) Distribution of the magnetic induction upon penetration into the superconducting state, 550 Oe and 5 K is shown. (c) Superposition of (a) and (b). (d) Different part of polished surface. (e) Remanent (trapped) flux after fc and turning field off. (f) Superposition of (d) and (e).

large as $200 \times 100 \mu\text{m}^2$. Sensitivity to the orientation of the light polarization plane with respect to the crystal structure serves as an additional indication that we are dealing with well ordered crystallites. Tetragonal symmetry of the unit cell suggests that the crystals should grow as plates with the ab -plane being the extended surface and the c -axis along the shortest dimension. We examined various cross-sections of the ≈ 5 mm diameter and 5 mm height pellets. Based on the thickness of extremely rectangular grains, we estimate the thickness of the plates to be as large as $30 \mu\text{m}$. The magnetic flux penetration is consistent with isotropic in-plane persistent current densities, further confirming that the large grains represent the ab -plane of the tetragonal crystallites.

We can correlate this microstructure with the ability of this superconductor to shield magnetic field and trap the flux. Figure 2(b) shows penetration of the magnetic flux into the

region imaged in figure 2(a) after zfc, whereas figure 2(e) shows remanent (trapped) flux in the region imaged in figure 2(d). Figures 2(c) and (f) are the superpositions of figures 2(a) and (b) and figures 2(d) and (e), respectively. The correspondence between good superconducting regions and the largest crystals is evident.

3.2. Supercurrent density

There are several ways to estimate the shielding current from the measurements of total magnetic moment. For a slab of dimensions $2w \times 2b \times 2d$ (magnetic field is along the d side and $w \leq b$) within the Bean model [19], the total magnetic moment, M , is given by $M = jwV[1 - w/(3b)]/2c$, where c is the speed of light, V is the sample volume and j is the persistent (Bean) current that results from vortex pinning (we avoid calling this quantity the ‘critical’ current, because it is significantly affected by the magnetic relaxation). In the present case, for a magnetic field parallel to the long side of a slab, $2d = 0.44$ cm, $2w = 0.07$ cm, $2b = 0.18$ cm and $V = 5.54 \times 10^{-3}$ cm³. Therefore, $j[\text{A cm}^{-2}] \simeq 1.2 \times 10^5 \times M[\text{emu}]$. Taking the maximum half-width of the full hysteresis loop, see inset to figure 3, at $H = 0$, $M_{\text{rem}}(5 \text{ K}) \simeq 0.2$ emu, we estimate $j(5 \text{ K}) \simeq 2.4 \times 10^4$ A cm⁻². Another way to estimate the shielding current density is to measure the field of full penetration [20], $H^* = 4wj(2\arctan(\eta) + \eta \ln(1 + \eta^{-2}))/c$, where $\eta = d/w$. The field of full penetration may be estimated from the minimum of the $M(H)$ loop. In our case, we have $\eta = 6.3$, $H^* \simeq 1100$ Oe and therefore $j \simeq 2.6 \times 10^4$ A cm⁻², which is close to the above estimate and implies that the superconducting fraction is close to 100%. To verify this conclusion we measured reversible (Meissner) $M(H)$ at small, ± 10 Oe, field span that showed no hysteresis. The overall shielding was then estimated from $4\pi\chi = 4\pi(1 - N)M/VH$, where $N = (1 + 2\eta)^{-1} \simeq 7.4 \times 10^{-2}$ is the demagnetization factor (we neglected the London penetration depth, λ , that enters via the λ/w correction and is thus irrelevant [21]). At 5 K we found $4\pi\chi = -0.98$, essentially perfect diamagnetism. Given the uncertainty in V and N , as well as the neglected λ we see that this sample exhibits close to 100% diamagnetic screening.

These results can be compared to local magnetic measurements. The persistent current may be evaluated from the measurements of the z -component of the magnetic induction on the slab’s top surface using magneto-optical imaging. Defining $\Delta B = |B_z(x = 0, z = d) - B_z(x = w, z = d)|$ and assuming a full critical state, we have [20]

$$\frac{\Delta B c}{4\tilde{j}\tilde{w}} = \eta \ln \frac{(1 + 4\eta^2)^2}{16\eta^3\sqrt{1 + \eta^2}} + 2 \arctan(2\eta) - \arctan(\eta) \quad (1)$$

where we use ‘ $\tilde{}$ ’ to refer to quantities estimated for the individual crystallites. In the present case, a rectangular crystallite of $2\tilde{w} = 70$ μm , $2\tilde{b} = 160$ μm and assuming thickness $2\tilde{d} = 30$ μm was analyzed. Therefore we have $\eta \simeq 30/70 \simeq 0.43$ and $\tilde{j}[\text{A cm}^{-2}] \simeq 529\Delta B$ [G]. With $\Delta B \simeq 605$ we estimate $\tilde{j}(5 \text{ K}) \simeq 3.2 \times 10^5$ A cm⁻². Clearly, there is about an order of magnitude difference from the estimate from bulk magnetization. The reason is simple: the critical state is established in each individual crystallite, not on the scale of the entire sample, and so there is no macroscopic Bean gradient of the magnetic induction. This is why local measurements on the scale of an individual grain are required. Note that if $2\tilde{d}$ were infinite, the conversion would be $\tilde{j} \simeq 455\Delta B$, and for smaller $2\tilde{d}$ we expect a larger conversion factor. Therefore, we provided the conservative estimate of the critical current.

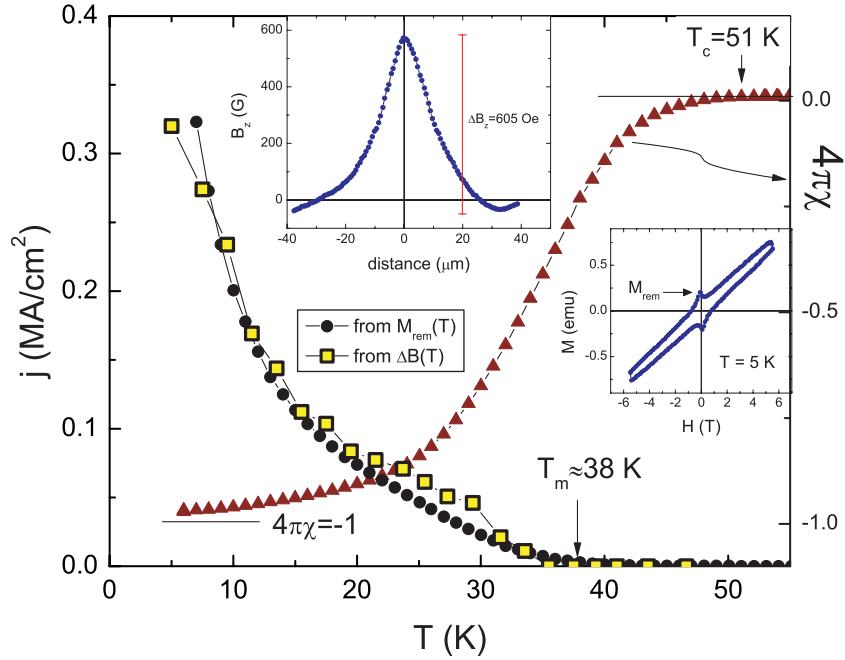


Figure 3. Persistent current density, j , estimated from local MO measurements (see text). For comparison, $M_{\text{rem}}(T)$ is scaled to match the amplitude (circles). Also shown is $4\pi\chi$ (triangles, right axis) to emphasize the ‘magnetic’ T_c . Upper inset shows example $B(r)$ and the definition of ΔB ; lower inset shows an $M(H)$ loop at 5 K.

Figure 3 summarizes the *local* and global measurements of the persistent current density in NFAOF. The squares show $\tilde{j}(T)$ obtained from ΔB as defined in the upper inset. For comparison, the full circles show the temperature dependence of the remanent magnetization rescaled by a single scaling factor to match the $\tilde{j}(T)$ obtained from local measurements. Suppose that the slab was split into crystallites of width $2\tilde{w}$ each carrying $\tilde{j} \sim 10^5 \text{ A cm}^{-2}$. A total of $n = w/\tilde{w}$ crystallites would produce a total magnetic moment of $\tilde{M} \sim n\tilde{j}\tilde{w}\tilde{V} \sim \tilde{j}\tilde{w}$. If we want this moment to match the observed M , then $\tilde{w} \sim wj/\tilde{j} \sim 0.1w$. With $w \simeq 350 \mu\text{m}$ we obtain a good agreement with the directly observed width of the crystallites, $\tilde{w} \sim 35 \mu\text{m}$. This yields an important conclusion: in our sample global magnetic measurements can be used to access intra-grain persistent current, but the estimated magnitudes will be about ten times lower.

Figure 3 also shows other important features. The triangles (right axes) show magnetic susceptibility, $4\pi\chi$, measured at $H = 10 \text{ Oe}$. The magnetic $T_c \simeq 51 \text{ K}$ and resistive $T_c \simeq 53 \text{ K}$ [17]. However, the $\tilde{j}(T)$ virtually vanishes above about 35 K. Remarkably, the order of magnitude and overall temperature dependence of $\tilde{j}(T)$ is quite similar to that observed in BSCCO-2212 [22] where there is a clear crossover above $\sim 30 \text{ K}$ associated with the decoupling of pancake vortices (3D \rightarrow 2D crossover) [23].

3.3. Magnetic relaxation

Given this last observation, we now turn to a discussion of the sample’s dynamic properties. Magnetic relaxation is a valuable tool for determining vortex-related parameters of a

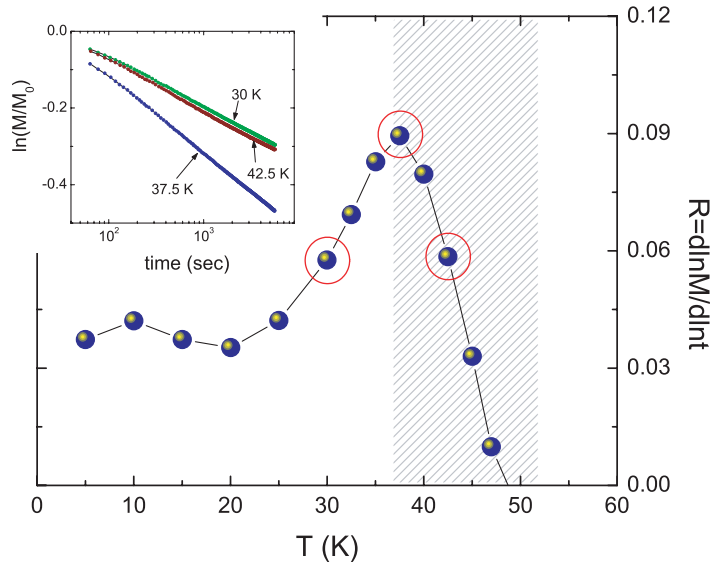


Figure 4. Logarithmic relaxation rate $R = d \ln M / d \ln t$ as a function of temperature. Inset shows time-dependent magnetization at three different temperatures below, at and above the peak in $R(T)$.

superconductor [24, 25]. The relaxation rate depends on the pinning parameters as well as the structure of the Abrikosov vortices and vortex lattice. A perfunctory inspection of the magnetic relaxation reveals a very large time dependence even at low temperatures. At 5 K, there is a 16% change of the total magnetic moment over 1.5 h; there is an even larger change of 38% at ~ 38 K. Whereas one can use sophisticated, nonlinear models, here it is sufficient to examine the logarithmic relaxation rate, $R = |d \ln M / d \ln t|$ which allows for comparison with other systems and is sample volume independent. Figure 4 shows a sharp increase of $R(T)$ and a peak at about ~ 38 K. It is worth noting that the temperature of the peak is in the same temperature range where the apparent persistent current (figure 3) drops almost to zero. Both observations are consistent with the vanishing of the barrier for vortex escape from the pinning potential at this temperature.

Comparing to cuprate high- T_c superconductors, we note that for different YBCO samples, including flux-grown, melt-processed crystals and films, $R(T)$ is confined to a narrow range between 0.02 and 0.04 and is fairly flat [25]. In contrast, for BSCCO, $R(T)$ exhibits a peak at the temperature of a crossover associated with pancake decoupling [23, 25]. Examining the magnetic field dependence of the relaxation rate we find that below 38 K it rapidly decreases with the increase of a magnetic field, despite the fact that the apparent irreversible magnetization is almost field independent above 1 kOe. This is consistent with the collective pinning and creep model in which the barrier for magnetic relaxation increases with increasing magnetic field due to the growth of vortex bundles.

The relaxation can also be measured in the individual crystallites. Figure 5 shows magnetic relaxation measured from a series of the snapshots taken initially at 150 ms intervals and later at 10 s intervals. Examples of two such snapshots are shown as insets. To estimate the persistent current, profiles of magnetic induction, shown in the upper inset, were measured along the indicated path and then converted into j as described above. The relaxation rate is quite

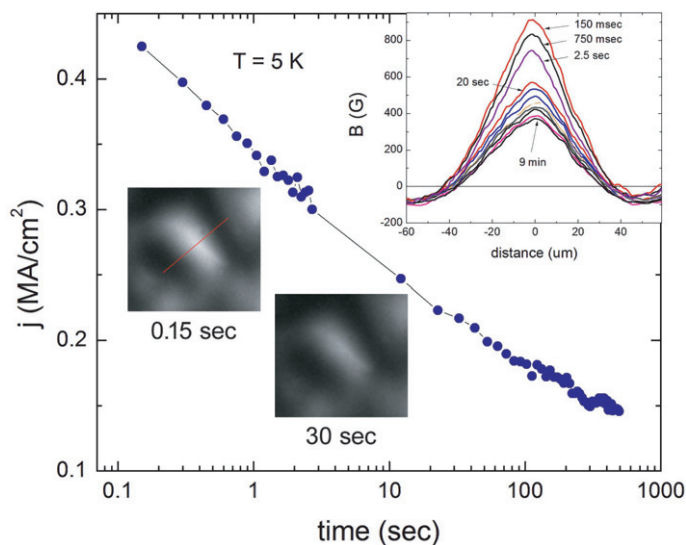


Figure 5. Relaxation of the persistent current measured from the decay of the magnetic induction profiles shown in the upper inset. Embedded images show two frames at 0.15 s and 30 s after the magnetic field was turned off. A line shows where profiles were taken.

high, approaching $R = 0.1$, which reflects the fact that the effective time constant depends on the sample size.

4. Conclusions

In conclusion, it seems plausible that the observed crossover in the pinning strength and magnetic relaxation rate at $T_m \approx 38$ K is associated with large thermal fluctuations that dominate the physics above that temperature. The physical processes at T_m could include melting of the still 3D vortex lattice or a crossover from 3D Josephson coupled pancake vortices to decoupled 2D pancakes, similar to that found at ~ 30 K in BSCCO [23]. Below T_m , the temperature and field dependence of the persistent current as well as its logarithmic relaxation rate are consistent with collective pinning and creep [24, 25]. The estimated current density, $\sim 10^5$ A cm $^{-2}$ is low enough for weak collective pinning to hold. Overall, the behavior of NFAOF is somewhere in between YBCO and BSCCO.

Acknowledgments

Discussions with S Bud'ko, V Kogan, M Tanatar, A Kaminskii, W McCallum, K Dennis and J Schmalian are greatly appreciated. We thank R T Gordon for help with preparing the manuscript. Work at the Ames Laboratory was supported by the Department of Energy-Basic Energy Sciences under Contract No. DE-AC02-07CH11358. RP acknowledges support from NSF grant number DMR-05-53285 and the Alfred P Sloan Foundation.

References

- [1] Kamihara Y *et al* 2008 *J. Am. Chem. Soc.* **130** 3296
- [2] Hai-Hu W *et al* 2008 *Europhys. Lett.* **82** 17009
- [3] Ni N *et al* 2008 *Phys. Rev. B* **78** 014507
- [4] Yan J Q *et al* 2008 *Phys. Rev. B* **78** 024516
- [5] Ni N *et al* 2008 *Phys. Rev. B* **78** 014523
- [6] Prozorov R *et al* 2008 *Phys. Rev. B* **78** 224506
- [7] Zhigadlo N D *et al* 2008 *J. Phys.: Condens. Matter* **20** 342202
- [8] Ren Z A *et al* 2008 *Europhys. Lett.* **82** 57002
- [9] Lv J-P and Chen Q-H 2008 *Phys. Rev. B* **78** 144507
- [10] Giovannetti G, Kumar S and van den Brink J 2008 *Physica B* **403** 3653
- [11] Grafe H J *et al* 2008 *Phys. Rev. Lett.* **101** 047003
- [12] Dubroka A *et al* 2008 *Phys. Rev. Lett.* **101** 097011
- [13] Yamamoto A *et al* 2008 *Appl. Phys. Lett.* **92** 252501
- [14] Weyeneth S *et al* 2009 *J. Supercond. Nov. Magn.* **22** doi: 10.1007/s10948-008-0413-1
Weyeneth S *et al* 2009 *J. Supercond. Nov. Magn.* **22** doi: 10.1007/s10948-009-0445-1
- [15] Balicas L *et al* 2008 arXiv:0809.4223
- [16] Okazaki R *et al* 2009 *Phys. Rev. B* **79** 064520
- [17] Martin C *et al* 2009 arXiv:0903.2220
- [18] Prozorov R 2007 *Phys. Rev. Lett.* **98** 257001
- [19] Bean C P 1964 *Rev. Mod. Phys.* **36** 31
- [20] Prozorov R 2008 arXiv:0811.0177
- [21] Prozorov R *et al* 2000 *Phys. Rev. B* **62** 115
- [22] Prozorov R *et al* 2003 *Phys. Rev. B* **67** 184501
- [23] Pradhan A K *et al* 1994 *Phys. Rev. B* **49** 12984
- [24] Blatter G *et al* 1994 *Rev. Mod. Phys.* **66** 1125
- [25] Yeshurun Y *et al* 1996 *Rev. Mod. Phys.* **68** 911